Korean J. Chem. Eng., 35(12), 2365-2378 (2018)
DOI: 10.1007/s11814-018-0158-x

pISSN: 0256-1115
eISSN: 1975-7220

Effect of vanadium surface density and structure in VOx/TiO_2 on selective catalytic reduction by NH_3

Jong Min Won, Min Su Kim, and Sung Chang Hong†

Department of Environmental Energy Systems Engineering, Kyonggi University,
94 San, Iui-dong, Yeongtong-gu, Suwon-si, Gyeonggi-do 16227, Korea
(*Received 28 March 2018 • accepted 29 September 2018*)

Abstract−We investigated the correlation between vanadium surface density and VOx structure species in the selective catalytic reduction of NOx by NH_3. The properties of the VOx/TiO_2 catalysts were investigated using physicochemical measurements, including BET, XRD, Raman spectroscopy, FE-TEM, UV-visible DRS, NH_3-TPD, H_2-TPR, O_2-On/Off. Catalysts were prepared using the wet impregnation method by supporting 1.0-3.0 wt% vanadium on TiO_2 thermally treated at various calcination temperatures. Through the above analysis, we found that VOx surface density was 3.4 VOx/nm^2, and the optimal V loading amounts were 2.0-2.5 wt% and the specific surface area was 65-80 m^2/g. In addition, it was confirmed that the optimal VOx surface density and formation of vanadium structure species correlated with the reaction activity depending on the V loading amounts and the specific surface area size.

Keywords: NOx, NH_3 SCR, VOx/WO_3/Titania, Surface Density, VOx Structure

INTRODUCTION

Nitrogen oxides (NOx) produced in various combustion engines using fossil fuels are one of the major air pollutants. Nitrogen oxides are mainly emitted from stationary pollution sources including industrial processes and power plants and mobile pollution sources including automobiles [1]. They form acid rain and photochemical smog and affect the greenhouse effects and destruction of the ozone layer [2,3]. Selective catalytic reduction (SCR) of NOx by NH_3 is a potential process for purification of exhaust gas. Techniques for NOx removal should satisfy the criteria of stability, economics and removal efficiency. Through this process, the NOx contained in the exhaust gas is converted into N_2 and H_2O through reactions with NH_3. This reaction is described in Eq. (1).

$$NO+4NH_3+O_2 \rightarrow 4N_2+6H_2O \quad (1)$$

Various attempts have been made to develop SCR catalysts. The VOx catalyst added on anatase TiO_2 shows a higher activity than the SCR reactions using various metal oxide catalysts [3]. Anatase TiO_2 is produced with various properties depending on the purpose of use by various manufacturers. The crystal phase of TiO_2 exhibits various physicochemical properties including specific surface area and particle size depending on the preparation methods. The activity varies depending on the vanadium loading amount present on the surface of the catalyst, but a measure is required to accurately interpret it. In general, the structure and physicochemical properties of the catalyst greatly affect the activity of the oxidation reaction [4-6]. Recently, studies on NH_3-SCR have been conducted mainly on promoter activity enhancement by addition of promoter metal. According to Liu et al. [7] the addition of Ce to the V_2O_5/TiO_2 catalyst improves the reaction activity depending on the redox characteristics. But, there are few studies on the analysis of the V structure species as the active metal on the catalyst surface. Giraud et al. [8] also studied the adsorption properties of ammonia by supporting V or V/W on V_2O_5/TiO_2 catalysts according to S-free TiO_2 or S-containing TiO_2. However, the above study has not been conducted to investigate the effect of the W-containing TiO_2 on the reaction characteristics of vanadium structure species. Likewise, the preparation method, temperature of thermal treatment, addition of promoter and properties of titania supports affect surface vanadium species and catalytic activity. In addition, even though various studies have been conducted on characterization of vanadia/titania catalysts prepared by various techniques, the structure of the surface vanadium species during the reaction has not been fully understood [9,10].

It has been proposed that various vanadium structures such as isolated vanadium species (in tetrahedral or octahedral coordination), polymeric-type species (spread over titanium oxide), and bulk vanadium oxide (either in amorphous or crystalline form) exist depending on the loading amounts on the surface of catalysts [11-14]. As the NH_3-SCR reaction proceeds, these structures exhibit various reactions [15,16]. NOx conversion, N_2 selectivity and properties of the surface activity point vary depending on the vanadium structure. In addition, it has been shown that the specific NH_3-SCR catalytic activity of the polymeric vanadate species was greater than that of the monomeric vanadyl species. However, the polymeric species increases the fluidity of the lattice oxygen in the reaction gas and exhibits high reduction ability.

Oxygen exists in various states on the surface of metal oxides in the catalyst. When oxygen molecules are adsorbed, they accept one electron and thus exist as the molecular ion in the form of O_2. When oxygen is converted to the atomic state by accepting another elec-

†To whom correspondence should be addressed.
E-mail: schong@kyonggi.ac.kr

tron, it is converted to oxygen ions and then absorbed onto the surface. When atomic oxygen ion accepts one more electron, it becomes oxygen ion and exists in a state absorbed to the metal oxide. However, when the oxygen forms oxide lattice by interacting with metal, the O^{2-} oxygen ion is called "lattice oxygen." The oxygen present in the active state of the metal oxide surface is called the "active oxygen species" [17]. In the SCR reaction, oxygen can participate in both gas phase and lattice oxygen reactions. In addition, there are some methods of measuring the effects of oxygen, such as a method of measuring the activity in the presence/absence of oxygen or a method of measuring the responses to oxygen supply pulse. Nevertheless, the pathway of oxygen involved in the reaction is not known yet.

The purpose of this study was to investigate the correlation between VOx surface density of the VOx/TiO_2 catalyst surface used in the NH_3-SCR reaction and VOx structure species. The catalysts used in this study were prepared by the wet-impregnation method. The catalysts were prepared on the same support depending on the vanadium loading amount and other catalysts were prepared on TiO_2 support which was prepared with the same vanadium loading amount by various calcination temperatures. The following analytical techniques were used to examine different denitrification efficiencies of the catalysts and to investigate the correlation between VOx surface density and vanadium structure species in the catalysts: N_2 adsorption-desorption with the BET method, XRD (X-ray Diffraction), FE-TEM (Field emission transmission electron microscopy), Raman spectroscopy, UV-visible diffuse reflectance spectroscopy (UV-vis DRS spectra), and temperature programmed reduction with hydrogen (H_2-TPR).

EXPERIMENTAL

1. Catalyst Preparation

TiO_2 (with W 8.0 wt%), purchased from Millennium Crystal Global Co., was in its titanium dioxide form, and the specific surface area of anatase TiO_2 was controlled according to various calcination temperatures. TiO_2 according to calcination temperatures was prepared by calcination 4 h in air after heating to the selected temperature at a rate of 10 °C/min. VOx/TiO_2 catalysts were prepared by the wet impregnation method using ammonium metavanadate (NH_4VO_3, Sigma-Aldrich Chemical Co.) based on 1.0-3.0 wt% vanadium and calcined TiO_2 powder. The calculated amount of NH_4VO_3 was dissolved in distilled water and heated to 60 °C. Since NH_4VO_3 has a low solubility, a small amount of oxalic acid ($(COOH)_2$, Sigma-Aldrich Chemical Co.) was slowly added to the aqueous solution of ammonium vanadium with stirring until pH 2.5 was reached to maintain pH.

When solution turned bright orange, a calculated amount of TiO_2 was added to the solution. The mixture was agitated as a slurry for 1 h, and then moisture was evaporated (N-N series, Eyela Co.) before drying overnight at 110 °C. The mixture was calcined in air for 4 h at 400 °C. Finally, samples were pressed, crushed, and sieved using 40-50 mesh (mean particle size 0.359 mm) to obtain suitable particles for the experiments. The resulting catalysts were labeled as xV/TiO_2, 2V/TiO_2-x00 where x was the vanadium loading amounts and x was the calcination temperatures for TiO_2 (with W), respectively. For example, a catalyst containing raw TiO_2 and 1.5 wt% vanadium loading amount was labeled as 1.5V/TiO_2 or TiO_2 calcined at 600 °C and 2 wt% vanadium loading amount was labeled as 2V/TiO_2-600.

2. Catalytic Characterization

The Brunauer-Emmett-Teller (BET) specific surface area of the TiO_2 supports was measured by physical nitrogen adsorption at −196 °C using an ASAP 2010C analyzer (Micromeritics Co.). The crystal structure of the calcined TiO_2 supports and xV/TiO_2, 2V/TiO_2-x00 catalysts was determined by XRD analysis using a D/Max-III (3 kW) diffractometer (Rigaku Co.). Cu Kα (λ=0.1506 nm) was used as a radiation source, and measurements were performed in the range of 2θ=10°-80° at a scanning rate of 4°/min. Field emission transmission electron microscopy (FE-TEM) images were recorded on a JEM-2100F (JEOL) microscope operating at acceleration voltage of 200 keV. Samples for the FE-TEM measurements were prepared by suspending ultrasonically treated catalyst powder in ethanol and placing a drop of the suspension onto a Cu grid. Raman spectra were recorded using a multichannel thermoelectric cooled (−70 °C) charge coupled device (CCD) detector under ambient condition using LabRAM HR UV/Vis/NIR (Horiba Co.) DRUV-vis spectra were analyzed by a Varian Cary-5000 spectrometer, with the use of DR (diffuse reflectance) equipment; the measuring range was 200-800 nm. Temperature programmed reduction with hydrogen (H_2-TPR) measurement was performed using 30 mg of the calcined catalysts from room temperature to 800 °C, at a heating rate of 10 °C/min in flowing H_2/He gas (10 : 90 vol/vol mixture with a total flow rate of 30 ml/min). Before H_2-TPR measurement, the catalyst was pretreated in a flow of 5.0 vol% O_2/Ar at 400 °C for 0.5 hr, followed by cooling 50 °C. The catalyst was placed in dilute hydrogen, and the consumption of hydrogen was monitored by Autochem 2920 (Micromeritics) by increasing the temperature to 800 °C at the rate of 10 °C/min.

The VOx surface density was calculated according to the following Eq. (2)

$$n_s(VOx nm^{-2}) = \frac{C_W \times N_A}{M_w \times S_{BET} \times 10^{18} (nm^2/m^2)} \quad (2)$$

In the above equation, C_w (g/g) is the vanadium content of catalyst, N_A the Avogadro's number (6.02×10^{23} mol^{-1}), M_w the molecular weight of vanadium (50.94 $gmol^{-1}$), and SBET (m^2g^{-1}) is the surface area of the catalysts.

3. Catalytic Activity Test

The SCR activity measurement was performed in a fixed-bed quartz reactor of 8 mm internal diameter. The typical reactant gases were fed to the reactor using a mass flow controller (MFC, MKS Co.). The reaction conditions were used as follows: 748 ppm NO, 55 ppm NO_2, NOx/NH_3 ratio 1.0, 3 vol% O_2, 6 vol% H_2O, and rest N_2. Approximately 0.15 g catalyst (40-50 mesh) was used for each run. Under ambient conditions, the total flow rate was 600 cc/min, and the gas hourly space velocity (GHSV) was 150,000 h^{-1}. Water vapor was generated by passing N_2 through a bubbler containing deionized water. The compositions of the feed gases and effluent streams were monitored continuously using on-line sensors with emission monitors: NDIR Gas analyzer (ZKJ-2, Fuji Electric Co.) for NO/NO_2 and (Fuji Electric Co.) for N_2O. Before the gas flowed

into the analyzers, moisture was removed by a moisture trap inside the chiller. All the data were collected starting from 60 min (steady state) at the selected temperature. From the concentration of the gases at the steady state, the conversion was calculated according to the following Eq. (3)

$$\text{NOx conversion (\%)} = \frac{[NO+NO_2]_{in}-[NO+NO_2+2N_2O]_{out}}{[NO+NO_2]_{in}}\times 100 \quad (3)$$

RESULTS AND DISCUSSION

1. NH_3-SCR Activity and Surface Density of VOx/TiO_2 Catalysts

The NH_3-SCR reaction activity was measured by using xV/TiO_2 catalysts which were prepared as below: xV/TiO_2 catalysts were calcined at 400 °C for 4 hours after various vanadium loading amounts such as 1.0-3.0 wt% were added to the same TiO_2 support, and $2V/TiO_2$-x00 catalysts were prepared by loading 2.0 wt% vanadium in the TiO_2 support, which was calcined at various calcination temperatures such as 400-800 °C. The results are shown in Fig. 1(a) and (b). To compare the NOx conversion of VOx/TiO_2 catalysts prepared by various preparation conditions, the reaction experiments were performed under the same conditions. The catalyst was heated to 400 °C prior to the reaction and then pretreated with 3 vol% O_2/N_2 gas for 1 hour. After that, a denitrification experiment was performed at various reaction temperatures such as 200-400 °C as the reaction gas including NOx (NO: 748 ppm, NO_2: 55 ppm) 803 ppm, NH_3/NOx ratio 1.0, O_2 3 vol% N_2 balance, H_2O 6 vol% was introduced at the space velocity of 150,000 hr^{-1}.

Results of the reaction activity of the xV/TiO_2 catalysts prepared with various vanadium loading amounts are shown in Fig. 1(a). As the properties of reaction activities, the denitrification efficiencies were compared in the high temperature region (400 °C) and the low temperature region (250 °C). The reaction activity of all catalysts prepared in the high temperature region was higher than 97% and there was no difference in the activity between catalysts. On the other hand, the catalysts prepared in the low temperature region showed the biggest difference in reaction activity at 250 °C. The NOx conversion efficiency of $2.5V/TiO_2$ was 80.12%. The activity tended to increase with increasing the vanadium loadings from 1.0 wt% to 2.5 wt%, but the efficiency of the catalyst prepared with the vanadium loading amounts of 3.0 wt% decreased to 78.87%. The reaction activity of $2V/TiO_2$-x00 catalysts loaded on the TiO_2 support prepared with the same vanadium loading amount at various calcination temperatures is shown in Fig. 1(b). In the case of high temperature region, there was no substantial difference in reaction activities of the catalysts prepared at various TiO_2 calcination temperatures. On the other hand, for the low temperature region, the reaction activity of $2V/TiO_2$-x00 catalyst showing the biggest difference in reaction activity at 250 °C exhibited similar reaction activities of 65% or higher at various calcination temperatures of 400-600 °C. However, the efficiency of catalysts prepared at calcination temperature of 700 °C and 800 °C gradually decreased to 63% and 49%, respectively.

Wachs et al. [18] reported that vanadium, which is active metal in VOx/TiO_2 catalyst being widely used as the SCR catalyst, was added in the catalyst to form the monolayer surface density, which

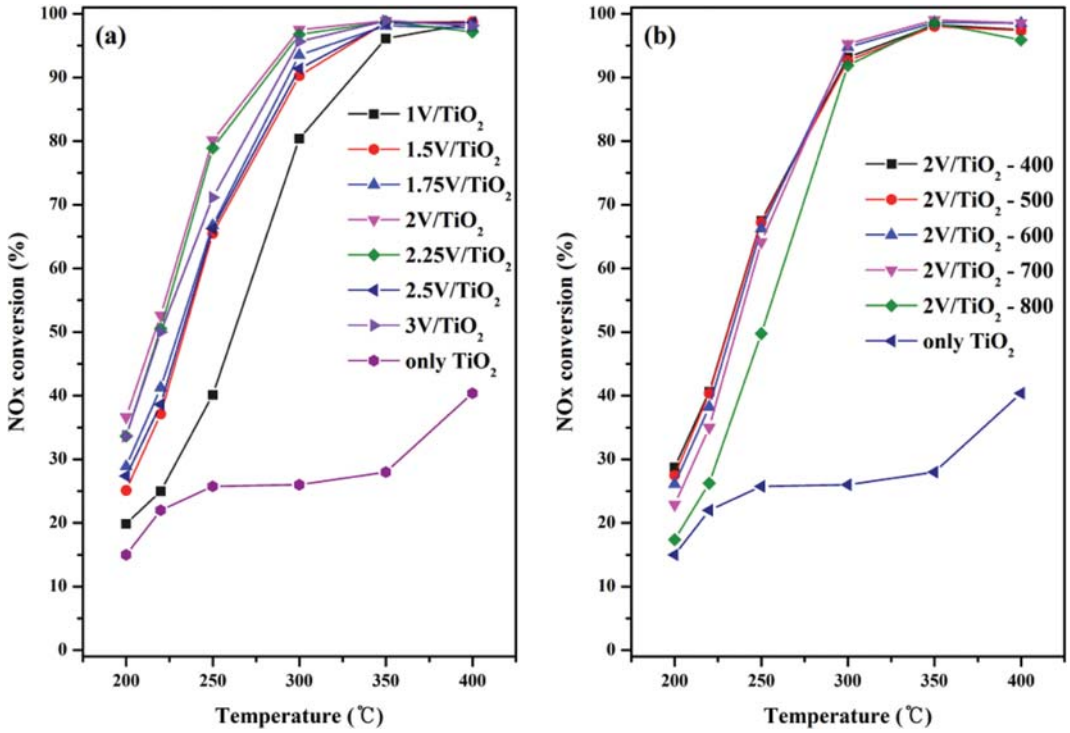

Fig. 1. NOx conversion of temperature on (a) xV/TiO_2 and (b) $2V/TiO_2$-x00 catalysts (Condition: NH_3/NOx ratio: 1.0, NO: 748 ppm, NO_2: 55 ppm, O_2 3%, H_2O 6%, S.V.: 150,000 hr^{-1}).

Table 1. BET properties of raw TiO_2, calcined TiO_2 and VOx surface density of xV/TiO_2, $2V/TiO_2$–x00 catalysts

Sample	S_{BET} (m^2/g)	Sample	VOx surface density (VOx/nm^2)	Sample	VOx surface density (VOx/nm^2)
Raw TiO_2	88.45	$1V/TiO_2$	1.33	$2V/TiO_2$-400	2.68
TiO_2-400	88.38	$1.5V/TiO_2$	2.05	$2V/TiO_2$-500	2.78
TiO_2-500	84.99	$1.75V/TiO_2$	2.33	$2V/TiO_2$-600	3.53
TiO_2-600	66.79	$2V/TiO_2$	2.67	$2V/TiO_2$-700	4.92
TiO_2-700	47.98	$2.25V/TiO_2$	3.01	$2V/TiO_2$-800	8.31
TiO_2-800	28.42	$2.5V/TiO_2$	3.34		
		$3V/TiO_2$	4.02		

was about 7.9 atoms/nm^2. VOx surface density means the number of atoms of vanadium oxide VOx which is added per specific surface area of vanadium, which is an active substance added to the carrier surface. According to Giakoumelou et al. [12] if excess vanadium, which is higher than appropriate VOx surface density is added, the distance between vanadium atoms produced on the surface of the catalyst would get very close and agglomeration would be caused by a thermal treatment process. Crystalline VOx species with increased crystallinity was produced by the above phenomenon. It reduced the denitrification efficiency of the entire NH_3-SCR by inhibiting the reduction ability of the catalyst. To investigate the correlation between reaction activity and VOx surface density of Vx/TiO_2 catalysts prepared with various vanadium loading amounts and $2V/TiO_2$-x00 catalysts controlling the specific surface of TiO_2 prepared with the same vanadium loading amounts, VOx surface density calculated from the specific surface is shown in Table 1.

As a result, the number of VOx atoms on the surface of the catalyst increased with increasing vanadium loading amounts. The surface density of VOx in xV/TiO_2 catalyst was increased from 1.33 VOx/nm^2 to 4.02 VOx/nm^2. In addition, the surface density of $2V/TiO_2$-x00 catalyst was also increased from 2.67 VOx/nm^2 to 8.31 VOx/nm^2.

The correlation between surface density of xV/TiO_2 catalyst and denitrification efficiency at various reaction temperatures such as 300, 250 and 200 °C is shown in Fig. 2. As a result, the denitrification efficiency at each reaction temperature tended to increase with increasing the surface density of the VOx/TiO_2 catalysts. However, the denitrification efficiency converged to the maximal denitrification efficiency at the VOx surface density of about 3.4 VOx/nm^2. In addition, when the VOx surface density was more than 3.4 VOx/nm^2, it showed a volcano plot in which the denitrification efficiency was decreased. It could be explained as below: The distance between V-V got closer with increasing vanadium loading amounts and the number of vanadium atoms on the surface of TiO_2 support of which specific surface was decreased at the calcination temperature. But, the agglomeration occurred while the distance between V-V atoms got close as much as the specific surface area was decreased. Thus, VOx surface density was thought to increase as well.

TiO_2 support being used in the SCR study was prepared by calcination of TiO_2 hydrolysis product which passed through the spray drying process from the initial titanic acid. XRD analysis was performed to observe the change of crystal phase of vanadium and TiO_2 of xV/TiO_2 and $2V/TiO_2$-x00 catalysts on the WOx/TiO_2 support containing tungsten among TiO_2 in which tungsten was present as a crystalline form after calcination. The results are shown in Fig. 3.

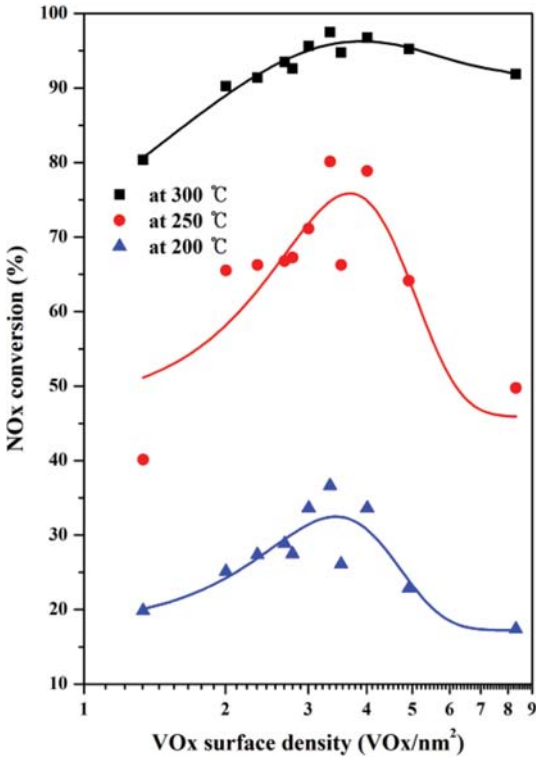

Fig. 2. Relationship between NOx conversion and VOx surface density of various VOx/TiO_2 catalysts.

As the (101) plane diffraction peak which was a main peak of anatase TiO_2 was observed at 2 Theta=25.28° in Fig. 3(a), it was found to have anatase TiO_2 crystalline structure. In addition, anatase TiO_2 peaks showing the crystalline structure were observed at Theta=37.34, 38.05, 38.75, 48.21, 54.00, 55.22, 62.74, 69.00, 70.4, 75.9° [19,20]. It has been known that W peak is observed at Theta= 23.67 and 33.85° [21], but the W peak was not developed in the xV/TiO_2 catalyst. The crystallinity of anatase TiO_2 increased, as non-crystalline titanic acid might become crystallization depending on thermal treatment conditions. In addition, anatase showing

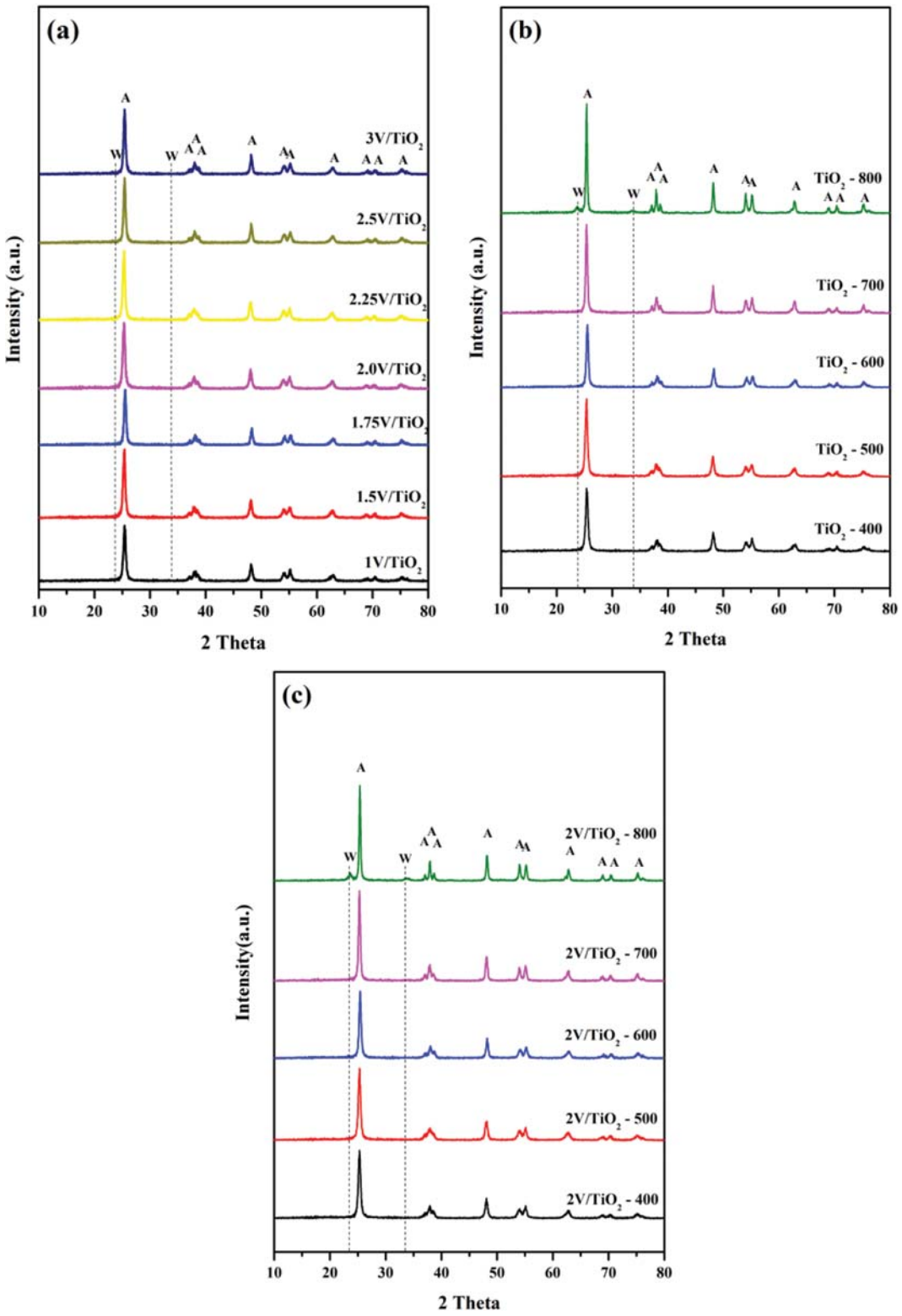

Fig. 3. XRD patterns of various VOx/TiO_2 catalysts: (a) xV/TiO_2, (b) TiO_2-x00, (c) 2V/TiO_2-x00.

metastability has been known to undergo phase transformation to rutile by heat at high temperature [22]. However, the crystalline structure depending on the vanadium loading amounts showed almost the same measurements without variations in this study. It was thought that the crystalline structure of anatase TiO_2 with strong bonds was not changed even though the vanadium loading amounts were increased in the preheated TiO_2. Fig. 3(b) shows that the crystallinity became more pronounced as the intensity of

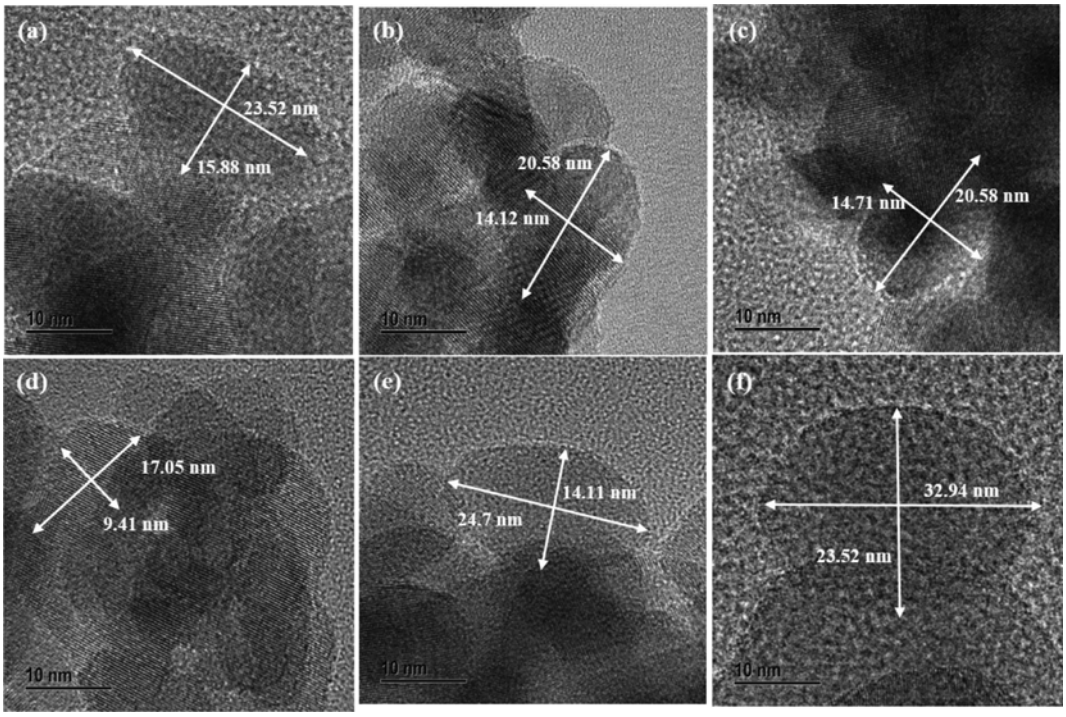

Fig. 4. TEM image of various VOx/TiO_2 catalysts: (a) 1V/TiO_2, (b) 2V/TiO_2, (c) 3V/TiO_2, (d) 2V/TiO_2-400, (e) 2V/TiO_2-600, (f) 2V/TiO_2-800.

anatase TiO_2 was more developed with increasing calcination temperature of anatase TiO_2. When 2V/TiO_2-x00 catalysts containing W went through the thermal treatment process at 800 °C, the W peak was observed. The specific surface area was decreased with increasing bonding force between Ti-Ti as the calcination temperature for TiO_2 was increased. The bonding strength between W-W was increased as much as the specific surface area of supports was decreased. As the calcination temperature increased, the crystal size of tungsten increased due to agglomeration phenomena caused by heat energy. According to the results of XRD analysis, it was found to have a W peak. However, it was difficult to identify crystalline micro-particles such as crystalline species caused by phase transition of TiO_2 anatase into rutile and agglomeration of vanadium, active metal. In this regard, TEM analysis was performed, because it enabled us to further analyze the microstructure of the catalysts. The results are shown in Fig. 4.

According to the results of TEM analysis, catalysts which were loaded with 1.0, 2.0, 3.0 wt% vanadium on the xV/TiO_2 catalysts which were prepared with various vanadium loading amounts on the same support were selected and measured. As the results, measurements of (a) 1V/TiO_2 23.52×15.88 nm, (b) 2V/TiO_2 20.58×14.12 nm, (c) 3V/TiO_2 20.58×14.71 nm were shown. Thus, it was found that increases in the vanadium loading amounts did not affect the catalyst particle size or crystallinity. 2V/TiO_2-x00 catalysts in which the same vanadium amount was loaded on the TiO_2 which was controlled by calcination temperatures of 400, 600, and 800 °C were selected and compared. As the results, measurements of (d) 2V/TiO_2-400 17.05×9.41 nm, (e) 2V/TiO_2-600 24.7×14.11 nm, (f) 2V/TiO_2-800 32.94×23.52 nm were shown. To control the specific surface area, it was found that the catalyst particle size or crystallinity increased in proportion to increases in the calcination temperature of TiO_2. It is thought to affect VOx surface density which was described above. With increasing calcination temperature, the crystal size of particles increased and the specific surface area decreased. Thus, VOx surface density in the catalysts is thought to increase.

2. Correlation of Surface Vanadium Species Structure and Surface Density

The structure of VOx on VOx/TiO_2 catalyst can be divided into monomeric vanadyl, polymeric vanadyl and crystalline V_2O_5 through Raman analysis. These materials have unique wavelength in Raman analysis. According to Bulushev et al. [23] VOx structure species of monomeric vanadyl and polymeric vanadyl have V-O bonds with different length. Especially, polymeric forms an oxygen bridge of V-O-V. The terminal bond (V=O) of monomeric VOx showed an absorption peak at about 1,030 cm^{-1}. On the other hand, the bridged bond (V-O-V) present only in the dimeric or polymeric VOx was observed in a wide range of 910-930 cm^{-1} and the terminal bond (V=O) showed an absorption peak at 1,016-1,030 cm^{-1}. The terminal bond of crystalline V_2O_5 showed an absorption peak at about 998 cm^{-1} [24-27]. Tungsten has also been known to exhibit absorption peaks at 981 and 805 cm^{-1}, and polymeric and crystalline WOx were observed through Raman analysis [28-30]. To examine the surface VOx type of xV/TiO_2 catalyst and 2V/TiO_2-x00 catalyst whose VOx surface density was calculated, Raman analysis was performed, and results are shown in Fig. 5. Detailed results, Fig. 5(a), are as follows: Raman peaks of xV/TiO_2 catalysts prepared with various vanadium loading amounts such as 1.0, 1.5, 2.0, 2.5, 3.0 wt% were analyzed. For 1V/TiO_2 catalyst prepared with low vanadium loading amount, polymeric tungsten and crystalline WOx peaks were clearly observed at 981 and 795 cm^{-1}, respectively. But, the intensity of tungsten peak of 1.5V/TiO_2 was substantially

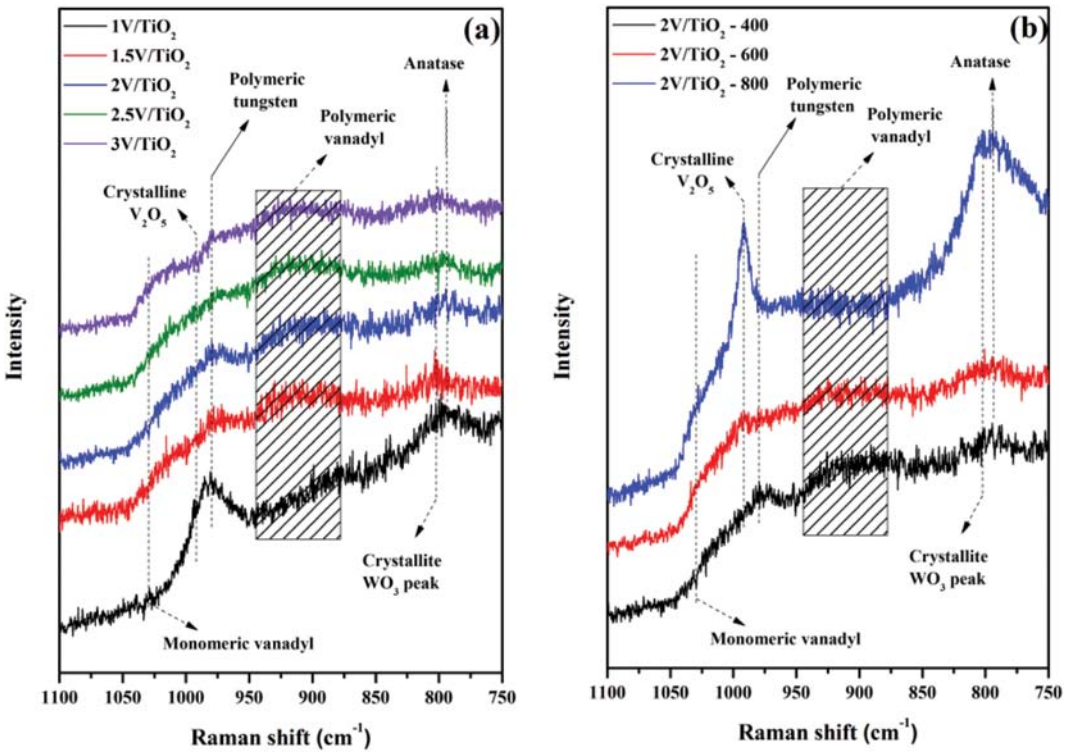

Fig. 5. Raman spectra of various VOx/TiO_2 catalysts: (a) xV/TiO_2, (b) 2V/TiO_2-x00.

reduced and a vanadium peak was accordingly observed. If the vanadium loading amount is more than 1.0 wt% and it is loaded on the TiO_2 support, tungsten sites in the support would be covered by vanadium and thus tungsten peaks would relatively decreased. In addition, when peaks of other catalysts from 1.5V/TiO_2 catalyst to 3V/TiO_2 catalyst were observed, polymeric vanadyl was mainly observed, but peaks of crystalline V_2O_5 were not observed. It was found that the crystalline VOx species was not formed, even though the vanadium loading amounts were increased in the initial TiO_2 support with high BET value by the wet impregnation method. Thus, the vanadium loading amounts could be controlled. In Fig. 5(b), 2V/TiO_2-x00 catalysts calcined at 400, 600, and 800 °C were selected and Raman peaks of the catalysts were analyzed. With increasing calcination temperature, it tended to increase from 2.67 VOx/nm^2 to 8.31 VOx/nm^2, as described in Table 1. In addition, BET of supports at calcination temperature of 400, 600, and 800 °C was 88.38, 66.79, and 28.41 m^2/g, respectively. It was found that 2V/TiO_2-400 catalyst had peaks of polymeric tungsten and crystalline WOx at 981 and 804 cm^{-1}, respectively. The intensity of polymeric tungsten in 2V/TiO_2-600 catalyst was substantially reduced. In addition, peaks of crystalline V_2O_5 and broad peaks of polymeric vanadyl were observed. In the 2V/TiO_2-800 catalyst, a broad peak of polymeric vanadyl was reduced, but a peak of the crystalline V_2O_5 was highly developed and peaks of anatase and crystalline WOx were also highly developed.

Based on the above results, the specific surface area of the TiO_2 support calcined at 600 °C or higher was 66.79 m^2/g. When 2 wt% or more vanadium was loaded on the catalysts with the specific surface area of 66.79 m^2/g or less, small amount of crystalline V_2O_5 was formed on the surface of the catalyst. Moreover, if the catalyst was calcined at 600 °C or higher, peaks of anatase of TiO_2 support (raw) and crystalline WO_3 would be developed and thus the crystallinity would be substantially increased due to occurrence of agglomeration caused by heat energy.

Based on the above results, crystalline V_2O_5 which decreased the denitrification efficiency in the VOx/TiO_2 catalyst was formed. It was also found that the formation of crystalline V_2O_5 could be controlled by the specific surface area of the TiO_2 support before vanadium was loaded. Thus, although the vanadium loading amounts were increased, the formation of crystalline V_2O_5 was not observed in the TiO_2 support with a large specific surface area. On the other hand, when the same amount of 2 wt% vanadium was loaded on the TiO_2 support with a small specific surface area, the formation of crystalline V_2O_5 began at BET=66.79 m^2/g. In this case, it would be difficult to control the vanadium loading amounts.

It is difficult to apply Raman analysis to the quantitative analysis of monomeric and polymeric VOx and analysis on low vanadium loading amounts. On the other hand, analytical methods enabling to analyze monomeric or polymeric morphology and structure species such as crystalline V_2O are using the DRUV-vis spectrum [11,31,32]. The DRUV-vis spectral method has some disadvantages in which it is difficult to interpret because the band of the target active metal is overlapped with the other band on which the support is absorbed. To overcome this disadvantage, Catana et al. [33] developed a method of obtaining a unique spectrum of VOx using a reference material as a carrier. This method is very useful for measuring VOx on various carriers. DRUV-vis spectroscopy provides useful information for the structural analy-

Table 2. DRUV-vis spectral data band assignments

DRUV-vis Band	λ max (nm)	Type of transition	Type of VOx species
Band 1	397-403	LMCT	Tetrahedral VO_4^{3-} and VO_3^-
Band 2	440	LMCT	Square pyramidal V_2O_5
Band 3	472	LMCT	Distorted octahedral $V_2O_6^{2-}$
Band 4	550	d-d	Square pyramidal V^{4+}
Band 5	668	d-d	Square pyramidal V^{4+}

sis of VOx species present on the surface of VOx/TiO_2 and is used for the quantitative analysis of monomeric or polymeric VOx [34-36]. The various VOx species were Tetrahedral VO_4^{3-}, VO_3^- depending on the structure and showed weak peaks at 397-403 nm (band 1). In addition, square pyramidal V_2O_5 species showed a weak peak at 440 nm (band 2). Distorted octahedral $V_2O_6^{2-}$ species showed a peak at 472 nm (band 3). V^{4+} species had a square pyramid shape and showed peaks at 550, 668 nm (bands 4, 5). In addition, the edge energy of the vanadium species was sensitive to coordination number and structure. Based on these properties, UV edge energies (Eg) of vanadium structure species were 2.72, 2.42, 2.22, 1.85 and 1.51 eV, respectively [11]. The λ max, type of transition and type of vanadate species at various bands are shown in Table 2.

According to Due-Hansen et al. [36] the *in situ* UV-vis spectra analysis of VOx-WOx/TiO_2 showed the maximal peak at around 650 nm and d-transition band was observed. It suggested that a peak was reduced by re-oxidation and then V^{4+} was generated. Thus, even though VOx structure was square pyramid, strong absorption of $V_2O_4(V^{4+})$ at high wavelength was caused by d-d orbital transition.

Fig. 6 shows the DRUV-vis spectra of the raw TiO_2, xV/TiO_2 catalysts prepared with various loading amounts, TiO_2-x00 support, and 2V/TiO_2-x00 catalysts by using $BaSO_4$ as a reference material. In Fig. 6(a), TiO_2 showed a band of strong charge transfer (CT) at 250-400 nm. On the other hand, the size of the bands tended to decrease at below 300 nm as the vanadium loading amounts increased. It was found that the peak was developed at 300-500 nm as the vanadium loading amounts increased. Fig. 6(b) shows the DRUV-vis spectra of the TiO_2-x00 which was the support prepared at various calcination temperatures by using $BaSO_4$ as a reference material. As a result, a band was observed at 250-400 nm and the intensity of the band tended to decrease with increasing calcination temperature. Fig. 6(c) shows the DRUV-vis spectra of the 2V/TiO_2-x00 catalyst in which the same vanadium loading amount was deposited on the TiO_2 prepared at various calcination temperatures. As a result, the intensity of the bands tended to decrease with increasing calcination temperature. In addition, some peaks were observed at 400-550 nm. Based on above results, a strong CT band appeared at 250-400 nm together with a weak VOx band at 400-550 nm. If $BaSO_4$ was used as a reference material, it would be difficult to interpret DRUV-vis spectrum results because peaks of TiO_2 and VOx would be overlapped [37].

Srinivas et al. [11] claimed that the spectrum of TiO_2 without metal can be used as a reference material for the VOx/TiO_2 DRUV-

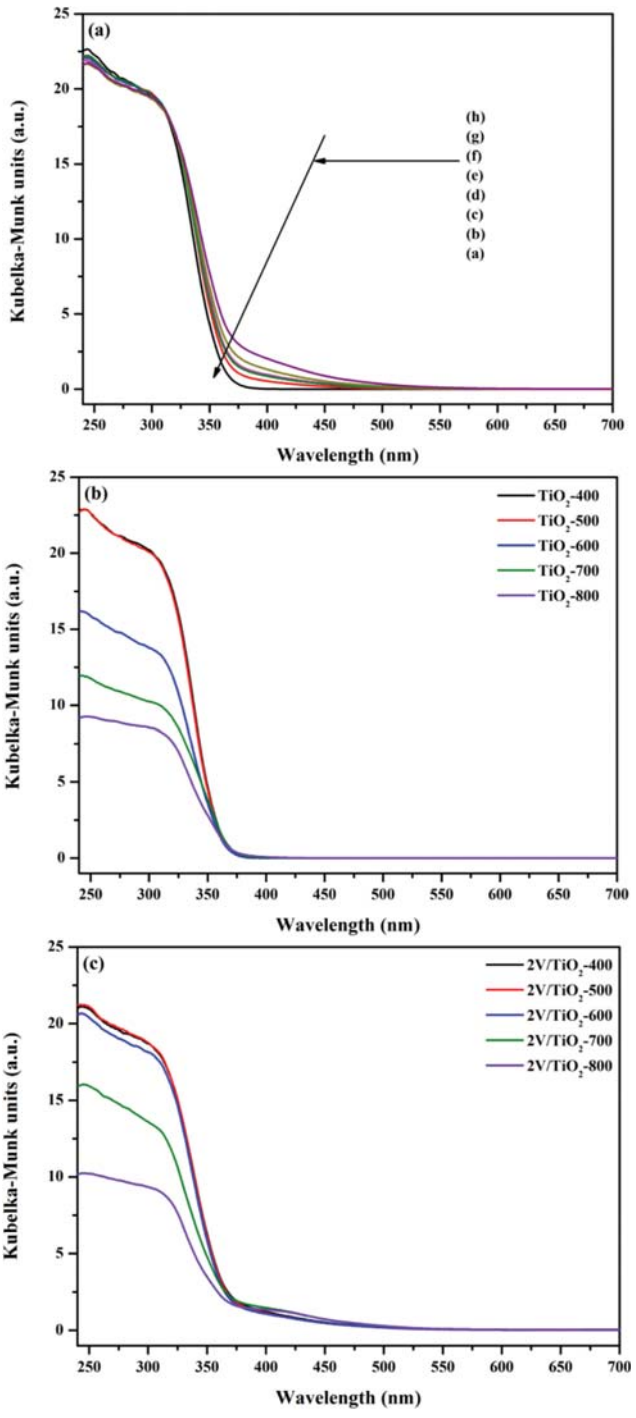

Fig. 6. DRUV-vis spectra of (a) raw TiO_2, xV/TiO_2, (b) TiO_2-x00, (c) 2V/TiO_2-x00 using $BaSO_4$ as a reference material.

vis spectroscopic analysis because DRUV-vis spectrum was the result of VOx rather than TiO_2. Thus, the spectra of raw TiO_2 and TiO_2 prepared at various calcination temperatures were used as a reference material to solve the issue of overlapping between TiO_2 and VOx in Fig. 6(a) and 6(b), respectively. The results of analysis on spectra of xV/TiO_2 catalyst and 2V/TiO_2-x00 catalysts are shown in Fig. 7.

Due to the VOx species dispersed on the TiO_2 support in each

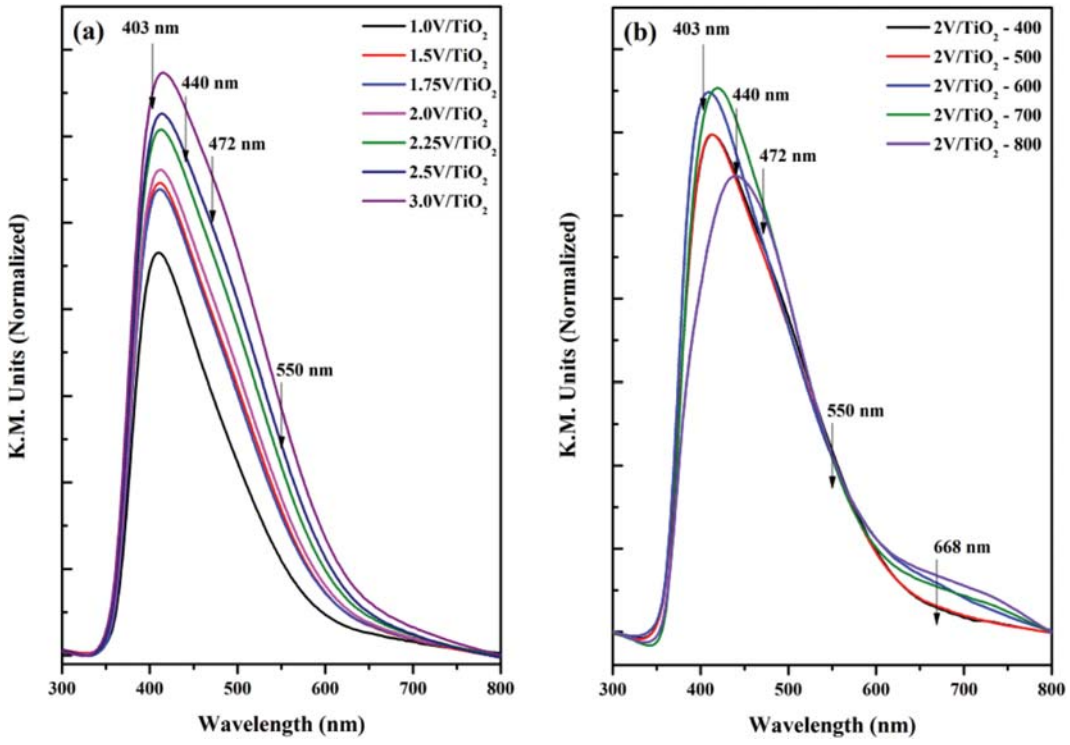

Fig. 7. DRUV-vis spectra of (a) xV/TiO_2, (b) 2V/TiO_2-x00 recorded against the support raw titania, calcined titania as a reference.

catalyst, DRUV-vis spectra showed asymmetric broad absorption peaks at 350-800 nm. This was a spectrum of only vanadium dispersed on the carrier, and it was possible to determine vanadium type and structure species. Detailed results are as follows: In Fig. 7(a), the size of entire peak was increased with increasing vanadium loading amounts. Areas of peaks at 403, 440, 471 and 550 nm seemed to gradually increase. In Fig. 7(b), the area of entire peak of 2V/TiO_2-x00 catalysts with the same vanadium loading

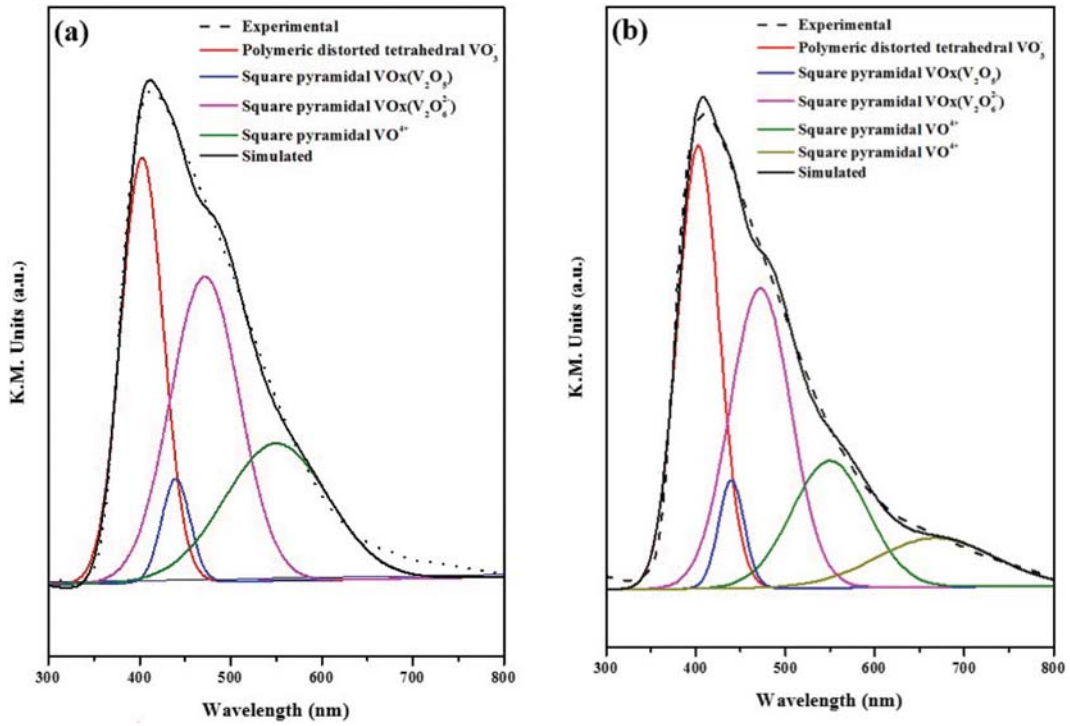

Fig. 8. Deconvoluted plots along with experimental and simulated DRUV-vis spectra for (a) xV/TiO_2, (b) 2V/TiO_2-x00.

amount seemed to be similar. In addition, with increasing calcination temperature, the position of peaks was changed. As the peak was shifted to a higher wavelength, the peak of the catalyst calcined at 600 °C or more was observed at 668 nm. The position of each peak indicates the VOx structure species on the surface of the catalyst. Type of vanadyl present on the catalysts was identified by performing peak fitting deconvolution of each catalyst. In addition, results of $2V/TiO_2$ (raw) and $2V/TiO_2$-600 are shown in Fig. 8(a) and (b), respectively.

Five bands representing the maximum value at 403(I), 440(II), 472(III), 550(IV) and 668(V) in DRUV-vis spectrum showing a wide asymmetric curve were deconvoluted. The ratios of the band and VOx structure species were derived by performing deconvolution of xV/TiO_2 and $2V/TiO_2$-x00 catalysts. As a result, the polymeric vanadyl ratio of $2.5V/TiO_2$ and $2V/TiO_2$-600 catalysts which had the VOx surface density of 3.4 VOx/nm^2 showing the optimal denitrification efficiency of NH_3-SCR was 0.309 and 0.333, respectively. Fig. 9 shows the correlation between the ratio of vanadium structure species and VOx surface density.

According to Kwon et al. [38] when a high amount was loaded to VOx/TiO_2, the concentration of the polymer VOx increased and the crystalline square pyramidal VOx continued to increase above a certain concentration. In addition, Giakoumelou et al. [12] reported that it was important to suppress crystalline V_2O_5 when VOx/TiO_2 was prepared, because vanadium aggregated to form crystalline V_2O_5, and crystalline V_2O_5 inhibited the reduction potential of the catalyst, thus reducing the SCR activity. According to Kompio et al. [39] vanadium loading amount and activity were proportionally increased when deposited as a single layer, and the formation of polymeric tetrahedral VO_3^- (band 1) varied depending on surface area of support and vanadium loading amounts.

As a result of this study, the ratio of crystalline VOx in xV/TiO_2 and $2V/TiO_2$-x00 catalysts at the VOx surface density of 3.4 VOx/nm^2 was the lowest and the ratio of polymeric VOx was the highest. In addition, square pyramidal VOx species gradually decreased below the optimal surface density of 3.4 VOx/nm^2 and it tended to increase above 3.4 VOx/nm^2. VOx surface density of VOx/TiO_2 could vary depending on surface area of support and vanadium loading amounts. Thus, VOx surface density can be used as a factor which determines the structure of VOx structure on the surface of the catalyst.

3. Correlation of Surface Vanadium Structure and Reactive Oxygen

The adsorption of ammonia in the SCR reaction is basically an important reaction characteristic. According to Busca et al. [40] and Amores et al. [41] anatase TiO_2 adsorbed ammonia on the Lewis acid site and ammonium ion on the V-OH site. It was reported that ammonia adsorbed on the Brönsted acid site was attributed to vanadium supported on TiO_2. The NH_3 adsorption/desorption experiments were conducted to express the amount of ammonia adsorbed on the catalyst surface and the strength of the acid sites [42]. Therefore, NH_3-TPD analysis of xV/TiO_2 catalyst and $2V/TiO_2$-x00 catalyst was performed to confirm these characteristics. Fig. 10(a) and (b), respectively.

The ammonia adsorption species, Lewis acid site, binds more strongly than the Brönsted acid site. On the other hand, temperatures below 200 °C can be classified into B acid sites, and peak temperatures can be classified into L acid sites [43]. The adsorp-

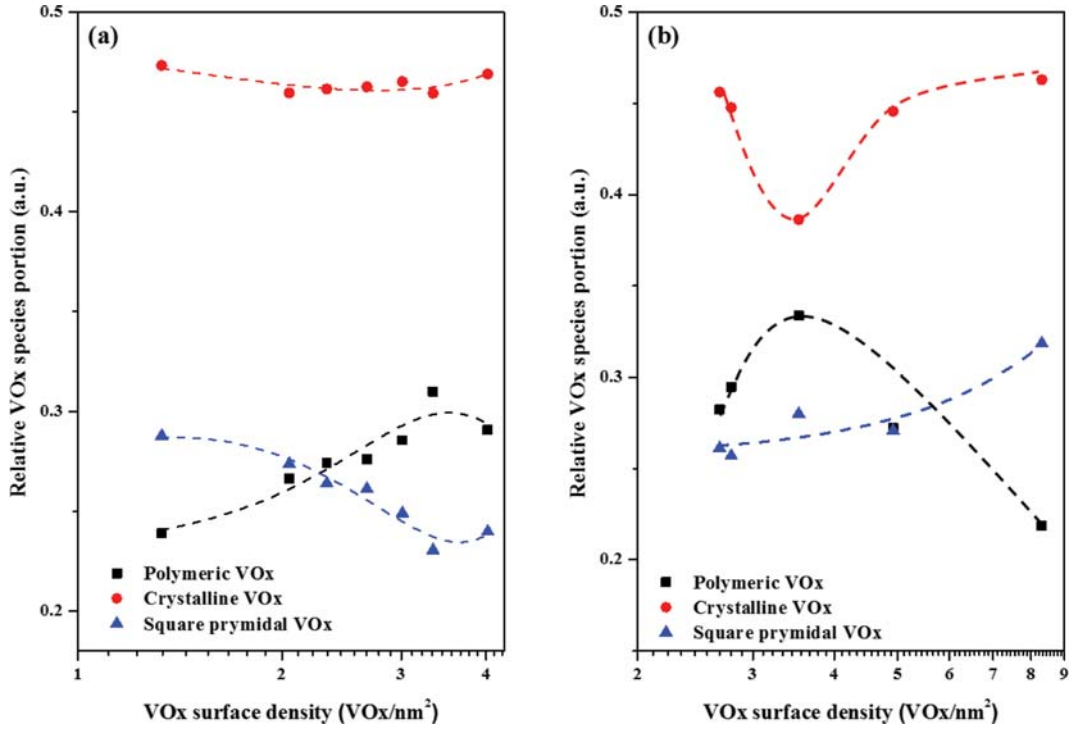

Fig. 9. Variation in the areas of the DRUV-vis bands corresponding to different VOx species in (a) xV/TiO_2, (b) $2V/TiO_2$-x00 as a function of VOx surface density.

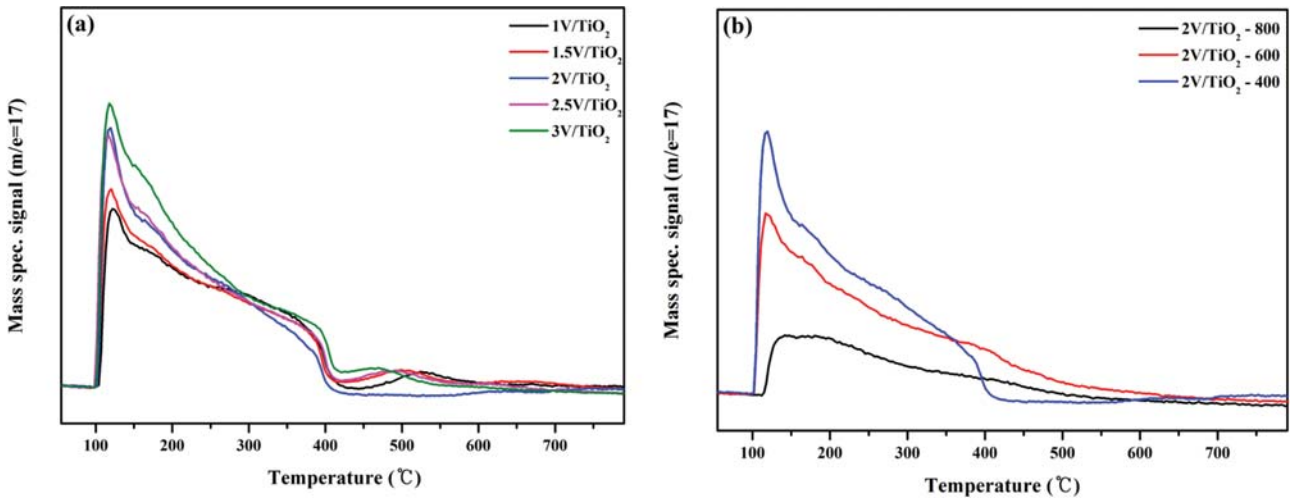

Fig. 10. NH_3-TPD profiles of VOx/TiO_2 catalysts: (a) xV/TiO_2, (b) 2V/TiO_2-x00.

tion amount of NH_3 on xV/TiO_2 catalyst increased as the loading amount increased. It is considered that the adsorption amount is increased in proportion to the increase in the number of NH_3 adsorbed sites as the vanadium content on the catalyst surface increases. On the other hand, in the case of 2V/TiO_2-x00 catalyst, the adsorption amount decreased as the temperature increased from 400 °C to 800 °C. This is because the 2V/TiO_2-600 catalyst showing the excellent denitration efficiency with the optimized surface density exhibited the NH_3 adsorption amount decreased. From these results, the amount of ammonia adsorption does not show a correlation with the reaction activity. It is considered that the vanadium structure species formed on the surface of the catalyst formed from the changed V surface density showed different reaction activity due to different characteristics.

The main reaction activity factors in NH_3-SCR are the oxidation/reduction action and oxidation state characteristics of the catalyst. In particular, it is known that the oxidation/reduction action plays an important role in the low temperature reaction having low activation energy [44,45].

Since participation of oxygen in the catalytic lattice may affect

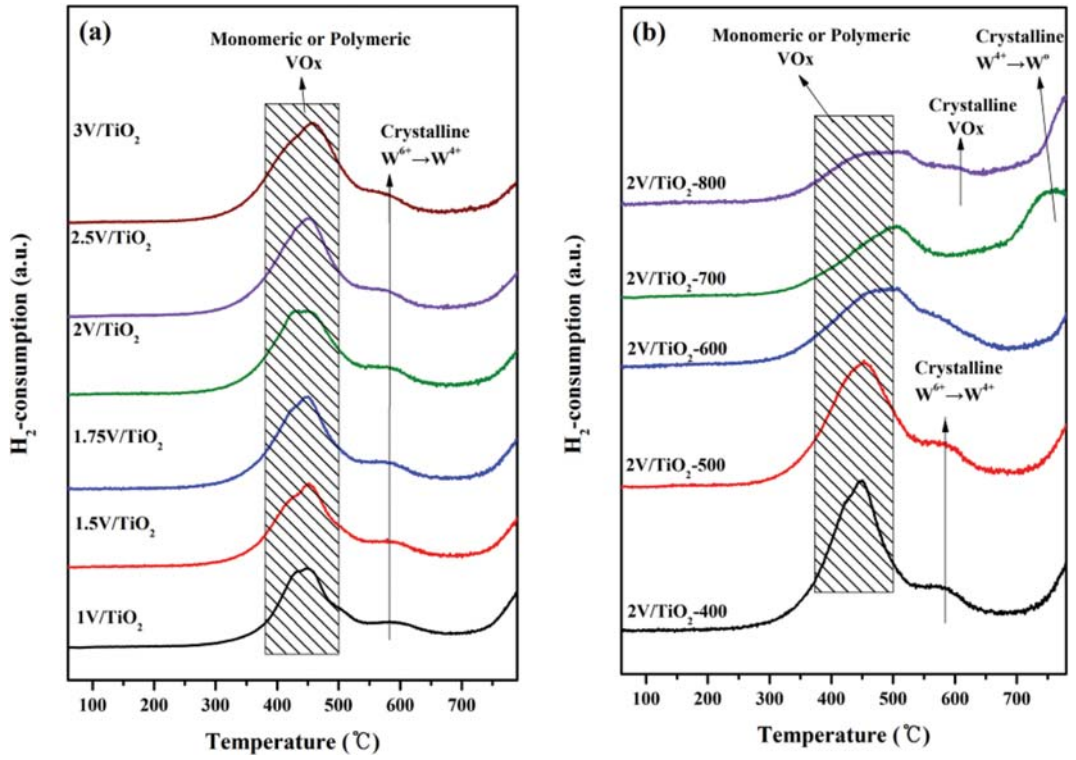

Fig. 11. H_2-TPR profiles of VOx/TiO_2 catalysts: (a) xV/TiO_2, (b) 2V/TiO_2-x00.

Table 3. H_2-consumption amount of xV/TiO_2, $2V/TiO_2$-x00 catalysts

Sample	H_2-consumption (mole/g)	Sample	H_2-consumption (mole/g)
$1V/TiO_2$	7.65	$2V/TiO_2$-400	9.31
$1.5V/TiO_2$	8.41	$2V/TiO_2$-500	8.83
$1.75V/TiO_2$	9.06	$2V/TiO_2$-600	5.91
$2V/TiO_2$	9.42	$2V/TiO_2$-700	4.37
$2.5V/TiO_2$	10.59	$2V/TiO_2$-800	4.00
$3V/TiO_2$	11.33		

the reduction ability, H_2-TPR analysis was performed to investigate quantitative analysis and effects of lattice oxygen. The position of the maximum reduction temperature (T max) in the H_2-TPR varied depending on the support type of the prepared catalyst and the vanadium loading amounts [46,47]. To identify these properties, we performed H_2-TPR analysis of xV/TiO_2 catalyst prepared by using the same support with various vanadium loading amounts and $2V/TiO_2$-x00 catalyst prepared at various calcination temperatures of the support with the same vanadium loading amount and compared the effects on hydrogen consumption amounts. The results are shown in Fig. 11(a) and (b).

Fig. 11(a) shows that H_2-consumption area of monomeric or polymeric VOx species [48,49] occurring at 370-500 °C was increased with increasing vanadium loading amounts. However, it was found that the position of maximum reduction temperature for the catalysts prepared with various vanadium loading amounts at the same calcination temperature was about 453 °C. Since the amount of W which already existed in the support was the same, the area of the crystalline W species [50] generated at 580 °C was almost the same. To analyze this more quantitatively, the area for H_2-consumption amount was calculated and shown in Table 3. As a result, the area increased proportionally from 7.65 mol/g to 11.33 mol/g as the vanadium loading amount was increased on the same support. However, the catalyst loaded with 3.0 wt% had a maximum consumption of 11.33 mol/g, but its NOx conversion efficiency was lower than that of the catalysts loaded with 2.5 wt% at low temperature. At this time, H_2-consumption was 10.59 mol/g. H_2-consumption of each catalyst did not show a direct correlation with NOx conversion efficiency. In Fig. 11(b), the amount of H_2 used for the reduction tended to decrease as the calcination temperature of TiO_2 increased, and the maximum reduction temperature was also increased. According to Giakoumelou et al. [12] the amount of H_2 used for the reduction of H_2-TPR of V/TiO_2 increased with increasing amount of vanadium, and the maximum reduction temperature also increased at the same time.

It is not related to the catalytic activity, but it is related to VOx existing on the surface of the catalyst such as a terminal bond (V=O), an anchoring bond (V-O-Ti) or a bridged bond (V-O-V). In addition, according to Roozeboon et al. [51] a large amount of H_2 consumption was observed due to the strong interaction between the support and the metal in an anchoring bond (V-O-Ti), which was mainly observed at the low vanadium amount. Oxygen was bound to vanadium existing in a bridged bond (V-O-V). H_2-TPR peak was observed at relatively high temperature due to weak interaction between the support and metal. H_2-TPR peak of Crystalline VOx was observed at high temperature.

We found here that the calcination temperature of the support was related to the variation of H_2 consumption peak indicating the structure species of the metal existing in the catalyst. In particular, with increasing calcination temperature, the maximum reduction temperature in the support calcined at 400 and 500 °C was developed at around 450 °C, but peaks with almost similar intensity were observed at 450 and 490 °C in the support calcined at 600 °C. As the temperature increased to 700 °C and 800 °C, a peak was highly developed at the maximum reduction temperature of 490 °C. In addition, the catalyst calcined at 800 °C showed a peak at around 620 °C. The reasoning is as follows: As the distance between V-V was reduced due to specific surface area, which decreased with increasing calcination temperature of the support, the amount of the active metal that could be bonded was increased, and thus VOx species was developed in the monomer VOx. In particular, crystalline VOx species in the catalyst calcined at 800 °C [52] was clearly observed at 620 °C. H_2-consumption peak of the catalysts calcined at 800 °C was observed at 700 °C. It has been known that there was a peak [53] of crystalline WOx existing in the support changing from 4^+ species to 0 species. The support catalyst calcined at 800 °C was shifted to 790 °C. As shown in the above results, H_2-consumption peak of the metal was shifted to high temperature or amount of consumption was decreased as the calcination temperature increased. It was thought to be caused by strong bonding force between metal and metal or metal and support in the catalyst.

According to the results of this study, the amount of hydrogen consumption calculated by H_2-TPR analysis had no direct correlation with NOx conversion efficiency, but it was a factor which could determine the amount of V on the surface of catalyst or VOx structure species by specific surface area of the support prior to V loading. Especially, the variation in the structure species of VOx was thought to be greatly affected by variation in specific surface area of the support rather than artificial variation in the Vanadium loading amounts in the same support.

The lattice oxygen in the catalyst has been shown to participate in the SCR reaction and is known to affect the oxidation/reduction properties of the catalyst [54,55]. The oxygen vacancies on the catalyst surface can diffuse back into the lattice, and lattice oxygen from the bulk can diffuse to the catalyst surface. When the oxygen supply is shut off, the catalyst can use a limited amount of lattice oxygen from the catalyst without re-oxidation. Without gaseous oxygen, the lattice oxygen from the catalyst is not re-oxidized, so the limited lattice oxygen inside the catalyst is eventually consumed. Re-oxidation through the flow of NO at low temperature is also considered to be difficult. To confirm the reactivity of the lattice oxygen bonded with the structural species which changes according to the surface density of vanadium, which is the active metal on the catalyst surface, the O_2 on/off study was performed. Fig. 12(a) and (b).

The O_2 on/off analyses were investigated on xV/TiO_2, $2V/TiO_2$-x00 catalysts. After NOx conversion reached the steady state following injection of NO and NH_3 at 250 °C, NOx conversion was observed for 1 hr after stopping the supply of oxygen and the activ-

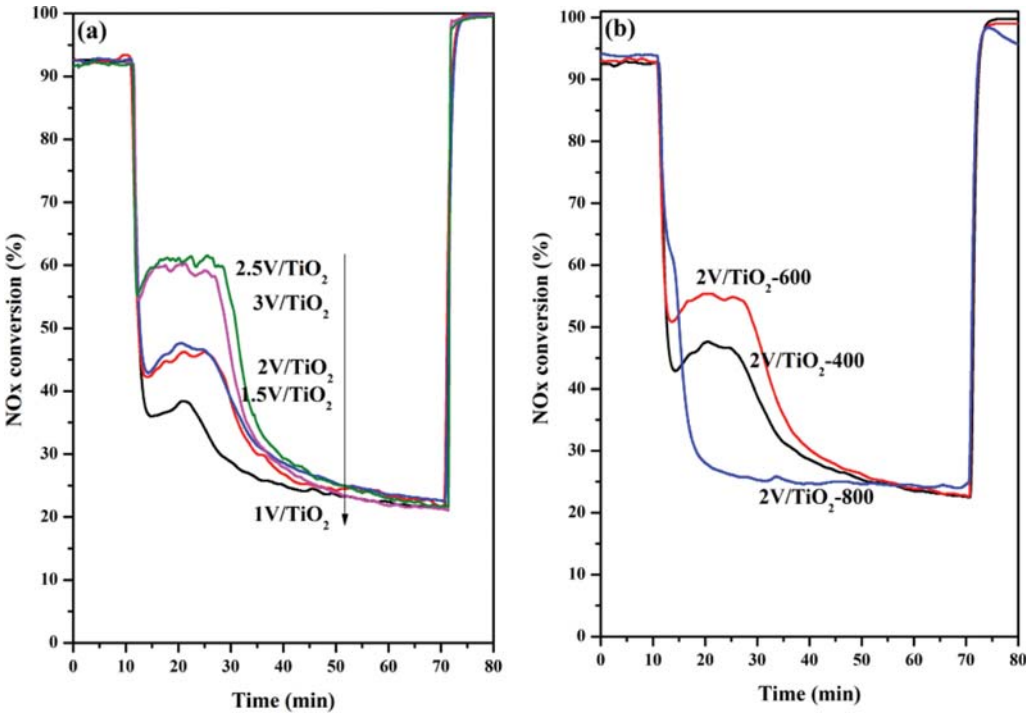

Fig. 12. Decline of NOx conversion over time shut of O_2 at 250 °C of VOx/TiO_2 catalysts: (a) xV/TiO_2, (b) 2V/TiO_2-x00 (Condition: NH_3/NOx ratio: 1.0, NO: 748 ppm, NO_2: 55 ppm, O_2 3%, S.V.: 20,000 hr^{-1}).

ity was later recovered upon supplying oxygen.

Experimental results show that the reaction rate at which the oxygen supply is cut off and the efficiency is reduced in the xV/TiO_2 catalyst is lowered to the same slope. On the other hand, the reaction activity was partially recovered as the vanadium loading was increased. It can be confirmed that the value represents the optimal value for the controlled V surface density and the denitrification efficiency area linearly according to the vanadium supporting amount of the catalyst surface or the specific surface area of TiO_2. From these results, it is considered that it is easy to use oxygen species which is formed when the surface density is optimum.

It can be seen that the polymeric VOx ratio according to the V surface density calculated in the previous study has a correlation with the lattice oxygen participating in the reaction. This means that as the polymeric VOx ratio increases, the amount of lattice oxygen involved in the reaction increases. This is because, unlike monomeric VOx species, polymeric VOx has cross-linking (V-O-V). Thereby, the lattice oxygen involved in the reaction is known to be provided from the V-O-V bond. The NH_3-SCR reaction mechanism follows the Eley-Rideal Langmuir-Hinshelwood mechanism [56]. In the Eley-Rideal reaction, NH_3 is absorbed by V^{5+}-OH (B acid site) and activated by the adjacent V^{5+}=O species. V^{5+}=O is regenerated by the reification of the V^{4+}=O species at redox sites [57]. The rate of SCR reaction is also known to be proportional to the amount of V^{5+}=O [58].

Polymeric VOx exhibits excellent catalytic activity due to enhanced activation during NH_3 adsorption by adjacent V^{5+}=O. The gaseous oxygen is important in the SCR, but the lattice oxygen is an important factor involved in the reaction. Thus, polymeric VOx species increase the lattice oxygen content of the reaction and exhibit excellent catalytic activity.

CONCLUSIONS

This study was conducted to investigate the correlation between VOx surface density and NH_3-SCR activity of the xV/TiO_2 catalyst prepared with various vanadium loading amounts on the same support and 2V/TiO_2-x00 catalyst prepared with the same vanadium loading amount on the TiO_2 support at various calcination temperatures. The VOx surface density varied greatly depending on the specific surface area and vanadium loading amounts on the TiO_2. The VOx surface density showing the maximum denitration efficiency was about 3.4 VOx/nm^2. Under the optimum conditions, the major vanadium structure species in the VOx/TiO_2 catalyst was polymeric VOx species, and thus the denitrification efficiency was expected to increase. VOx/TiO_2 catalyst showing the maximum denitrification efficiency seemed to be used as a factor controlling VOx structure on the surface by using VOx surface density. In addition, we can select TiO_2 having a suitable specific surface area to determine the maximum activity when the vanadium loading amount is determined, and we can determine vanadium loading amount in TiO_2 when the specific surface area is selected.

ACKNOWLEDGEMENTS

This work was supported by the Center for Environmentally Friendly Vehicle (CEFV) through Global-Top Project, funded by Korea Ministry of Environment (MOE) (2016002080004).

REFERENCES

1. G. Qi and R. T. Yang, *J. Catal.*, **217**, 434 (2003).
2. P. Granger and V. I. Parvulescu, *Chem. Rev.*, **111**, 3155 (2011).
3. Z. Liu and S. I. Woo, *Catal. Rev. Sci. Eng.*, **48**, 43 (2006).
4. F. Cavani, C. Cortelli, A. Frattini, B. Panzacchi, V. Ravaglia, F. Trifirò, C. Fumagalli,R. Leanza and G. Mazzoni, *Catal. Today*, **118**, 298 (2006).
5. U. G. Nielsen, N.-Y. Topsøe, M. Brorson, J. Skibsted and H. J. Jakobsen, *J. Am. Chem. Soc.*, **126**, 4926 (2004).
6. A. Bellifa, D. Lahcene, Y. N. Tchenar, A. Choukchou-Braham, R. Bachir, S. Bedrane and C. Kappenstein, *Appl. Catal. A: Gen.*, **305**, 1 (2006).
7. Z. Liu, S. Zhang, J. Li, J. Zhu and L. Ma, *Appl. Catal. B: Environ.*, **158-159**, 11 (2014).
8. F. Giraud, C. Geantet, N. Guihaume, S. Loridant, S. Gros, L. Porcheron, M. Kanniche and D. Bianchi, *J. Phys. Chem. C*, **119**, 15401 (2015).
9. I. Georgiadou, Ch. Papadopoulou, H. K. Matralis, G. A. Voyiatzis, A. Lycourghiotis and Ch. Kordulis, *J. Phys. Chem. B*, **102**, 8459 (1998).
10. J. P. Balikdjian, A. Davidson, S. Launay, H. Eckert and M. Che, *J. Phys. Chem. B*, **104**, 8931 (2000).
11. D. Srinivas, W. F. Hölderich, S. Kujath, M. H. Valkenberg, T. Raja, L. Saikia, R. Hinze and V. Ramaswamy, *J. Catal.*, **259**, 165 (2008).
12. I. Giakoumelou, C. Fountzoula, C. Kordulis and S. Boghosian, *J. Catal.*, **239**, 1 (2006).
13. F. Tang, K. Zhuang, F. Yang, L. Yang, B. Xu, J. Qiu and Y. Fan, *Chin. J. Catal.*, **33**, 933 (2012).
14. Z. Wu, V. Schwartz, M. Li, A. J. Rondinone and S. H. Overbury, *J. Phys. Chem. Lett.*, **3**, 1517 (2012).
15. L. Lietti, I. Nova and P. Forzatti, *Top. Catal.*, **11-12**, 111 (2000).
16. Y. Peng, C. Wang and J. Li, *Appl. Catal. B: Environ.*, **144**, 538 (2014).
17. M. A. Bañares, L. J. Alemany, M. C. Jiménez, M. A. Larrubia, F. Delgado, M. L. Granados, A. Martinez-Arias and J. M. Blasco, *J. Solid State Chem.*, **124**, 69 (1996).
18. I. E. Wachs, *Catal. Today*, **27**, 437 (1996).
19. J. Engweiler, J. Harf and A. Baiker, *J. Catal.*, **159**, 259 (1996).
20. M. Kobayashi and K. Miyoshi, *Appl. Catal. B: Environ.*, **72**, 253 (2007).
21. G. D. Panagiotou, T. Petsi, K. Bourikas, C. Kordulis and A. Lycourghiotis, *J. Catal.*, **262**, 266 (2009).
22. R. D. Shannon and J. A. Pask, *J. Amer. Cer. Soc.*, **48**, 391 (2006).
23. D. A. Bulushev, L. Kiwi-Minsker, F. Rainone and A. Renken, *J. Catal.*, **205**, 115 (2002).
24. G. Busca, *J. Raman Spec.*, **33**, 348 (2002).
25. M. A. Bañares and I. E. Wachs, *J. Raman Spec.*, **33**, 359 (2002).
26. G. T. Went, S. T. Oyama and A. T. Bell, *J. Phys. Chem.*, **94**, 4240 (1990).
27. A. Christodoulakis, M. Machli, A. A. Lemonidou and S. Boghosian, *J. Catal.*, **222**, 293 (2004).
28. J. Engweiler, J. Harf and A. Baiker, *J. Catal.*, **159**, 259 (1996).
29. M. Kobayashi and K. Miyoshi, *Appl. Catal. B: Environ.*, **72**, 253 (2007).
30. G. D. Panagiotou, T. Petsi, K. Bourikas, C. Kordulis and A. Lycourghiotis, *J. Catal.*, **262**, 266 (2009).
31. R. Bulánek, L. Čapek, M. Setnička and P. Čičmanec, *J. Phys. Chem. C*, **115**, 12430 (2011).
32. N. Moussa and A. Ghorbel, *Appl. Surf. Sci.*, **255**, 2270 (2008).
33. G. Catana, R. R. Rao, B. M. Weckhuysen, P. Van Der Voort, E. Vansant and R. A. Schoonheydt, *J. Phys. Chem. B*, **102**, 8005 (1998).
34. D. Wei, H. Wang, X. Feng, W. T. Chueh, P. Ravikovitch, M. Lyubovsky, C. Li, T. Takeguchi and G. L. Haller, *J. Phys. Chem. B*, **103**, 2113 (1999).
35. J. M. Miller and L. J. Lakshmi, *J. Mol. Catal. A Chem.*, **144**, 451 (1999).
36. J. Due-Hansen, S. B. Rasmussen, E. Mikolajska, M. A. Bañares, P. Ávila and R. Fehrmann, *Appl. Catal. B: Environ.*, **107**, 340 (2011).
37. E. C. Alyea, L. J. Lakshmi and Z. Ju, *Langmuir*, **13**, 5621 (1997).
38. D. W. Kwon, K. H. Park and S. C. Hong, *Appl. Catal. A Gen.*, **499**, 1 (2015).
39. P. G. W. A. Kompio, A. Brückner, F. Hipler, G. Auer, E. Löffler and W. Grünert, *J. Catal.*, **286**, 237 (2012).
40. S. Meiqing, L. Chenxu, W. Jianqiang, X. Lili, W. Wulin and W. Jun, *RSC Adv.*, **5**, 35155 (2015).
41. R. R. Kumar, K. N. Rao, K. Rajanna and A. R. Phani, *Mater. Lett.*, **106**, 164 (2013).
42. M. M. Salman, P. A. Kumar and H. H. Phil, *Appl. Catal. B: Environ.*, **152-153**, 28 (2014).
43. Z. Hun, H. Weiliang, L. Gongxuan, L. Jiangyin, T. Zhicheng and Z. Xinping, *Appl. Surf. Sci.*, **379**, 316 (2016).
44. L. G. Pinaeva, A. P. Suknev, A. A. Budneva, E. A. Paukshtis and B. S. Bal'zhinimaev, *J. Catal.*, **193**, 145 (2000).
45. L. Lietti, G. Ramis, F. Berti, G. Toledo, D. Robba, G. Busca and P. Forzatti, *Catal. Today*, **42**, 101 (1998).
46. B. E. Handy, A. Baiker, M. Schraml-Marth and A. Wokaun, *J. Catal.*, **133**, 1 (1992).
47. S. Martinez, R. Morales, M. G. C. Galindo, A. G. Rodriguez and B. E. Handy, *Thermochim. Acta.*, **434**, 74 (2005).
48. A. J. Shi, X. Q. Wang, T. Yu and M. Q. Shen, *Appl. Catal. B*, **106**, 359 (2011).
49. C. Z. Wang, S. J. Yang, H. Z. Chang, Y. Peng and J. H. Li, *Chem. Eng. J.*, **225**, 520 (2013).
50. C. Z. Sun, L. H. Dong, W. J. Yu, L. C. Liu, H. Li, F. Gao, L. Dong and Y. Chen, *J. Mol. Catal.* A, **346**, 29 (2011).
51. F. Roozeboom, M. C. Mittelmeijer-Hazeleger, J. A. Moulijn, J. Medema, V. H. J. De Beer and P. H. J. Gellings, *J. Phys. Chem.*, **84**, 2783 (1980).
52. S. S. R. Putluru, L. Schill, A. Godiksen, R. Poreddy, S. Mossin, A. D. Jensen and R. Fehrmann, *Appl. Catal. B*, **183**, 282 (2016).
53. C. Wang, S. Yang, H. Chang, Y. Peng and J. Li, *Chem. Eng. J.*, **225**, 520 (2013).
54. L. Lietti, P. Forzatti and F. Bregani, *Ind. Eng. Chem. Res.*, **35**, 3884 (1996).
55. M. D. Amiridis, I. E. Wachs, G. Deo, J. M. Jeng and D. S. Kim, *J. Catal.*, **161**, 247 (1996).
56. N. Y. Topsøe, M. Anstrom and J. A. Dumesic, *Catal. Lett.*, **76**, 11 (2001).
57. M. Inomata, A. Miyamoto and Y. Murakami, *J. Catal.*, **62**, 140 (1980).
58. A. Miyamoto, Y. Yamazaki, M. Inomata and Y. Kurakami, *J. Phys. Chem.*, **85**, 2366 (1981).